Published in final edited form as:
Nat Neurosci. 2012 November ; 15(11): 1581–1589. doi:10.1038/nn.3241.

Divergence of visual channels in the inner retina

Hiroki Asari and **Markus Meister**
Department of Molecular and Cellular Biology and Center for Brain Science, Harvard University, Cambridge, Massachusetts 02138

Abstract

Bipolar cells (BCs) form parallel channels that carry visual signals from the outer to the inner retina. Each BC type is thought to carry a distinct visual message to select types of amacrine cells (ACs) and ganglion cells (GCs). However, the number of GC types exceeds that of BCs providing their input, suggesting that BC signals diversify on transmission to GCs. Here we explored in the salamander retina how signals from individual BCs feed into multiple GCs, and found that each BC could evoke distinct responses among GCs, differing in kinetics, adaptation, and rectification properties. This signal divergence results primarily from interactions with ACs that allow each BC to send distinct signals to its target GCs. Our results indicate that individual BC-GC connections have distinct transfer functions. This expands the number of visual channels in the inner retina and enhances the computational power and feature selectivity of early visual processing.

Introduction

The visual system processes light information by encoding and separating signals into many different channels. These operations begin in the bipolar cells (BCs) of the retina[1]. Bipolar cells are the secondary neurons, extending their dendrites and axons towards the outer and the inner retina, respectively, and they constitute the only conduit for transmitting the signals from photoreceptors to retinal ganglion cells (GCs) and amacrine cells (ACs)[2]. There are ~10 types of BCs in a vertebrate retina[3,4], and previous studies suggest that they form parallel channels where each BC type carries a distinct type of visual information[5]. Bipolar cells differ in morphology, in particular by the ramification pattern of dendrites[6] and the stratification of axonal arbors[3,4]. They have also been divided physiologically into “ON” and “OFF” response types, and within each of these groups one further distinguishes “transient” and “sustained” types based on their visual response characteristics[7]. Such functional differentiation results from connections to specific photoreceptors[8], the intrinsic properties of BCs such as their membrane receptors and channels[9,10], and inhibitory circuitry involving ACs in the inner retina[11–13].

Beyond separating the visual image into parallel channels, BCs carry out important roles through their transmission to GCs[1,14]. First, some BC synapses appear to be strongly rectifying — transmitting depolarization but not hyperpolarization — which leads to prominent nonlinearities in the responses of GCs, such as a pronounced sensitivity to pattern motion[15–17]. Other GCs respond more linearly[18], presumably drawing on BC synapses with less rectification. Second, some important nonlinearities arise through the interaction with ACs at the BC terminal. For example, the direction-selectivity of GCs is largely determined

Corresponding author: Markus Meister, meister@caltech.edu.
Present address (both authors): Division of Biology, California Institute of Technology, Pasadena, CA 91125

Author contributions: H.A. and M.M. designed the study and wrote the manuscript. H.A. performed experiments and analysis.

Competing interests: The authors declare no competing financial interests.

by presynaptic inhibition of BC inputs[19]. Third, BC synapses can undergo strong activity-dependent depression[20–23], and this short-term plasticity has been invoked as a mechanism for adaptation in certain GC responses[14,24]. Thus the function of BC-GC transmission has emerged as a key determinant of retinal computation.

The diversity of functions that have been assigned to BCs — the combination of stimulus filtering, nonlinearities, and plasticity — easily exceeds the number of distinct BC pathways. Indeed, the typical retina contains ~20 types of GCs[2]. Because each of the 10 BC types tiles the visual field with little overlap[25], a complete coverage by GCs therefore requires divergence from individual BCs to multiple GCs. This raises the question how those BC signals become diversified.

To address this issue, we studied divergence and convergence of transmission from BCs to GCs. We gained control of individual BCs in the salamander retina with sharp electrodes; simultaneously we recorded the firing in an entire field of surrounding GCs with an extracellular multielectrode array; in addition we modulated the AC network pharmacologically and stimulated the photoreceptors with patterns of light. Here we report that individual BCs distribute very distinct signals to different GCs. Interactions with ACs were essential for diversifying the temporal dynamics and adaptation properties of the signals, but not for other characteristics such as the degree of rectification. We also found that different outputs from each BC were modulated individually by ACs; thus signals to some target GCs were suppressed while those to others were unaffected, or even enhanced by disinhibition. Taken together, the results suggest that visual information undergoes dramatic divergence and convergence during transmission in the inner retina, and that considerable computation takes place at each BC-GC connection.

Results

To explore how each bipolar cell (BC) signal is distributed downstream, we intracellularly manipulated the activity of individual BCs in the isolated salamander retina (Fig. 1a, b), and recorded simultaneously the spiking activity of many surrounding ganglion cells (GCs; Fig. 1c, d). Frequently depolarization of a BC via current injection elicited spikes in GCs nearby (Fig. 1d), including those of different cell types (Supplementary Fig. 1). These sign-preserving responses in GCs likely arise through excitatory transmission from BCs. Other GCs were inhibited by BC depolarization, and we confirmed by pharmacological block of inhibition that this sign inversion arises from interposed amacrine cells (ACs; Supplementary Fig. 2). While it is reassuring that the actions of a single BC can be measured even across intervening neurons, the present study will focus on sign-preserving transmission to GCs.

Some of the sign-preserving responses were observed at great distances, up to ~1 mm from the stimulated BC. Given that the combined radius of BC terminal fields and GC dendritic fields is ~0.35 mm[3,26,27], these effects cannot arise from a monosynaptic connection. Such long-range connections were greatly attenuated when we applied a gap junction blocker (Supplementary Data), suggesting that signals propagate laterally through electrical junctions among neurons in the inner retina[26,28]. To exclude such patently polysynaptic effects, we further restricted the analysis to BC-GC pairs separated by ≤0.35 mm.

With these methods in place, we set out to characterize the diversity of signal transmission from BCs to GCs. For the reasons detailed above, we focused the approach on the following four aspects of BC-GC connections: (1) the dynamics of the GC response; (2) adaptation in GC responses across repeated BC depolarizations; (3) rectification of signal transmission to GCs; and (4) the gating of BC-GC signaling by ACs.

Dynamics

By examining the postsynaptic responses, we found considerable divergence and convergence of distinct BC signals. First, the same BC could evoke very different GC responses. For example, depolarization of a single BC elicited a sustained response in one GC but a sharply transient response in another GC (Fig. 2a). This indicates that the signals acquire their distinct dynamics at or after the BC-GC transmission. Second, a single GC could produce distinct responses to inputs from different BCs. After serially impaling several BCs, we encountered some GCs with a sustained response to one BC but a transient response to another BC (Fig. 2b). This indicates that the distinct dynamics arise at or before the BC-GC transmission. Apparently the transmission dynamics are specified neither by the presynaptic BCs nor by the postsynaptic GCs, but are determined at each individual BC-GC connection.

How substantial is this diversity in the output from individual BCs? To assess this quantitatively, we examined for each BC-GC connection the time course of GC firing on BC depolarization. We found that more than two-thirds of all BCs had significant variation in the peak latency among their connections to target GCs (Fig. 2c). Furthermore, the variation among the outputs from a single BC explained about two-thirds of the total variation across all the BC-GC connections. Since the BCs were sampled blindly from all cell types by the sharp electrode, it appears that the variation across cell types is less significant than the variation across the outputs of a single BC. Similarly, many GCs showed diversity among their BC inputs (Fig. 2d).

Visual signals thus differentiate in their dynamics not only at BC dendrites in the outer retina[7,10] but also on transmission from BCs to GCs in the inner retina, and before they are integrated by the GCs. This may involve a combination of pre- and post-synaptic mechanisms that are private to the individual BC-GC connections. One explanation of such diversity involves the function of inhibitory interneurons. For example, the transient responses could arise as a result of feedback or feedforward inhibition via ACs[11–13]. Another possible explanation is that individual synapses have different pre- or post-synaptic mechanisms, for instance, by using different receptor types[29,30]. We distinguished these alternatives by pharmacological methods. Following a block of inhibitory transmission via γ-aminobutyric acid (GABA) and glycine, the peak evoked firing rates increased in almost all GCs (Fig. 3c), as would be expected from a general loss of inhibition. This was accompanied by changes in the dynamics of the response. Unexpectedly, however, the dynamics of transient and sustained responses were altered in opposite directions. Following the inhibitory block, the formerly transient responses peaked later (Fig. 3a), whereas the formerly sustained responses peaked earlier (Fig. 3b). Thus the overall diversity in the GC response kinetics evoked by single BCs decreased significantly after elimination of AC circuits (Fig. 3d).

How can these bidirectional changes in dynamics be explained? Given the large increase in the evoked firing rate, one would generally expect a faster decline of the response due to synaptic fatigue and thus a shorter time to peak. For example, because tonic presynaptic inhibition prevents synaptic depletion[20,21,31,32], the pharmacological block of such inhibition would speed up the postsynaptic GC response to BC depolarization (Fig. 4b). But clearly this is not the only effect at work, since the formerly transient responses become more extended in time. One explanation for transient responses is that feedback or feedforward inhibition can truncate synaptic transmission shortly after onset of the GC response[11–13]. With such a microcircuit at the BC-GC connection, the loss of inhibition will lead to a longer peak latency (Fig. 4a, c).

Below we will elaborate on possible mechanisms that shape synaptic transmission from BCs. Regardless of the details, however, it appears that distinct microcircuits with inhibitory ACs are involved in regulating the dynamics of individual BC-GC connections, and that even a single BC engages quite different AC microcircuits at its various synapses.

Adaptation

Following repeated exposure to the same stimulus, many GCs change their response properties over time. Previous studies suggest that events at the BC terminal contribute to these visual adaptations in GC responses[22–24]. We thus examined whether GC responses evoked by single BC inputs change over consequtive trials (Fig. 5). Specifically, we alternately delivered 1 s of depolarizing and hyperpolarizing currents into individual BCs with 2 s intervals (Fig. 1d), and analyzed slow changes in the peak rate and latency of the GC responses. To avoid confusion between spontaneous and evoked spikes, we selected those GCs that had low spontaneous firing rates (≤1 Hz) and high evoked rates (≥5 Hz).

In the course of many repeated trials, some GCs desensitized, in that their responses became weaker and slower (Fig. 5a). By contrast, responses of other GCs did not change significantly (Fig. 5b), even though they all received inputs from the same BC. Interestingly, slow changes in the peak rate or in the latency could occur independently of each other (Fig. 5c, d). Compiling results from many such experiments, one gains a view of the broad diversity of adaptive behaviors, including both desensitization and sensitization, even in transmission from a single BC. Indeed, the variation arising among the connections of individual BCs explained most of the total variation in the adaptive behavior of the response latency, and about two-thirds for changes of the peak rate (Fig. 5e).

To examine the contribution of AC circuits, we again blocked inhibitory synaptic transmission pharmacologically. Surprisingly we found that the sensitizing or stable responses were largely turned into desensitizing ones (Fig. 5f, g): Almost all BC-GC connections now showed a gradual decline in the peak firing rate, with less diversity than prior to the block. Again, it appears that diverse AC circuits are responsible for much of the variation in behavior of BC-GC connections, even on the slow time scale of adaptation.

While the above experiments show diverse adaptive behaviors among the output connections of one BC, does the same diversity apply among the inputs of a given GC? For example, an inactivating sodium conductance contributes to slow desensitization at the level of spike generation[33,34], which should affect every BC input to that GC equally. Similarly the sensitizing responses of certain GCs have been explained with a circuit model that affects all the BC inputs[35]. To test this notion, we drove the same GC by stimulating two different BCs intracellularly. We found multiple cases where the GC adapted to inputs from one BC but not to those from another BC (Fig. 6b), even though the nonadapting responses were sometimes stronger than the adapting ones (Fig. 6a).

To further examine if adaptation to inputs from one BC occurs independently of the other, we drove a single BC with current injection, and many other BCs with a visual stimulus presented far from the impaled BC (Fig. 6c–e). Over a 10-s train of current pulses into the single BC, most GCs desensitized strongly (Fig. 6d), and often the response vanished completely (Fig. 6c). If this adaptation originated in a general loss of sensitivity after the GC integrates its synaptic currents[33,34], that should affect the response to all of the BC inputs. Instead, the GC responses to the light-evoked BC pathway did not change at all (Fig. 6e). This shows that the adaptation arises within the input pathway from a single BC. Combined with the above results on divergence from a single BC, we conclude that desensitization and sensitization are specific to a given BC-GC connection but not attributable to global changes in either the presynaptic or the postsynaptic neuron.

Rectification

Under stimuli of moderate strength, BC responses can be well described by a linear function of the light intensity[36,37]. By contrast, many GCs show highly nonlinear responses under those same stimulus conditions[15,16], and the effect has been attributed to rectification at the transmission from BCs to GCs[14,17]. Indeed we generally found a strong asymmetry in GC responses (e.g., Fig. 2): BC depolarization excited the GC much more than hyperpolarization inhibited it. Because many GCs had low spontaneous firing rates, however, this asymmetry could result from a cellular nonlinearity of spike generation in the GC, rather than synaptic rectification. To focus on the BC-GC transmission properties, we selected GCs with sufficiently high spontaneous firing rates (≥1 Hz) so that we could resolve a decrease as well as an increase of the firing rates. For those GCs, we examined the effects of BC currents of either polarity, and asked if the transmission was rectified or not. To this end, we used a rectification index that measures the relative efficacy of BC depolarization and hyperpolarization in changing the GC spiking activity (see Methods).

In general, BC depolarization and hyperpolarization had opposite effects on any given GC (Fig. 7); one leading to an increase of the firing rate and the other to a decrease. However, the relative strength varied over a wide range (Fig. 7b). For some GCs, only BC depolarization was effective (Fig. 7a, bottom), suggesting a rectifying transmission with the index distributed around unity. In others, depolarization and hyperpolarization had comparable effects in opposite directions (Fig. 7a, top), indicating nonrectifying transmission with the index close to zero. For nonrectifying connections, we frequently observed rebound responses — an increase in firing at the offset of BC hyperpolarization — whereas these were seen only rarely for rectifying connections (Supplementary Fig. 3). Because a given BC can make both rectifying and nonrectifying transmission to different targets (Fig. 7a), that same neuron can contribute to fundamentally different visual computations. Here we found that ~40% of the total variation of the rectification index arose from the diversity among the outputs from individual BCs (Fig. 7b).

Blocking inhibitory transmission did not affect the degree of rectification in BC-GC connections. Neither the rectification index nor the observed frequency of rectifying and nonrectifying responses changed significantly following the pharmacological block (Fig. 7b, d). Even without the contribution of ACs, the same BC could thus send both rectified and nonrectified signals to different GCs (Fig. 7c). This indicates that the signal rectification is intrinsic to individual BC-GC connections, perhaps depending on the baseline levels of calcium and vesicle release rates at the presynaptic BC terminals[38,39] (Supplementary Fig. 3).

Gating

We have observed that signals from ACs can strongly affect transmission at individual BC-GC connections (Figs. 3–5). But so far these AC signals were only evoked by the intracellularly stimulated BC. In general, ACs receive stimulation from a broader region of the visual field, and multiple ACs at different locations are involved in modulating BC-GC connections[14,19,40]. To explore the details of this modulation, we proceeded to drive the AC circuits independently by a visual stimulus, while monitoring their effect on transmission from individual BCs.

Specifically, we projected on the retina a randomly moving grating, but excluded the receptive field center of the target BC and GCs (see Methods). The stimulus by itself did not affect the baseline activity of the GCs (Fig. 8a and Supplementary Figs. 4b and 5), indicating that they did not receive any excitatory inputs directly from the light-driven BCs, and we selected these GCs for subsequent analysis. In contrast, this visual stimulus does

drive neurons in the periphery, including polyaxonal ACs whose processes are long enough to interact with the selected BC and GCs[17,24,40]. By combining such visual stimulation and single BC current injection, we were thus able to examine how light-driven ACs modify the GC responses to the current-driven BCs.

The background visual stimulation had diverse effects on BC-GC transmission. For some GCs the response to BC depolarization was suppressed (Fig. 8a, left), for others enhanced (Fig. 8a, right), and unaffected for the rest (Fig. 8b). Effects of opposite sign were observed even for transmission from the same BC (Fig. 8a, b). Of the total variation in these gating effects from distant stimuli, about 60% originated in diversity among connections from individual BCs (Fig. 8b). Similarly there was diversity among inputs converging onto a given GC: The same GC could experience suppression for one BC input but not for another (Fig. 8c and Supplementary Fig. 4b).

A block of inhibitory transmission from ACs eliminated these effects of peripheral visual stimulation (Fig. 8d and Supplementary Fig. 5). This means that ACs mediate both the observed suppression and enhancement of BC transmission, the latter presumably through disinhibition via serial AC connections[41]. We thus conclude that the gating of BC signals by distant stimuli occurs independently at each BC-GC connection, and that ACs innervate these synapses in a way that allows the selective switching of each connection.

Discussion

To examine how bipolar cell (BC) signals feed into ganglion cells (GCs), we simultaneously recorded from many GCs while manipulating individual BCs intracellularly, the associated amacrine cells (ACs) pharmacologically, and the surrounding circuits visually (Fig. 1). We found considerable divergence and convergence of diverse excitatory signals from BCs to GCs, indicating that individual BC-GC connections have distinct transfer functions despite their close proximity. First, a single BC could elicit sustained responses in some GCs but sharply transient responses in others (Fig. 2). Such diverse kinetics of signal transmission resulted largely from inhibitory circuits involving ACs (Figs. 3 and 4). Second, distinct modes of adaptation were found in transmission from individual BCs, demonstrated by slow changes of the response amplitude and latency over time (Figs. 5 and 6). Again this diversity was shaped by AC circuits. Third, synapses of the same BC differ considerably in their degree of rectification. This feature appears to be intrinsic to a given BC-GC connection without the contribution of AC circuits (Fig. 7 and Supplementary Fig. 3). Finally, BC-GC connections were individually modulated by ACs; some were suppressed while others were enhanced (Fig. 8 and Supplementary Figs. 4 and 5). Taken together, our results emphasize the diverse modes of BC-GC transmission and how it may be tuned by ACs.

Putative mechanisms for the diversity among BC synapses

What are the synaptic mechanisms for this diversity among the signals from a single BC? At this point we can only speculate, but there are some plausible candidates. In most BCs, across many species, the axon branches in a tree with many synaptic terminals near the tips[3,6,17,25,26] (Fig. 1b). Furthermore, ACs contact the BC specifically at its terminals, often in direct proximity to the glutamate release sites[11,42]. Thus it is tempting to identify the BC terminal as the key compartment that controls the BC-GC connection. This requires that different terminals be sufficiently isolated electrically or with respect to their calcium signals. Even within a terminal, there is evidence of presynaptic specializations that might differentially control transmission to different postsynaptic partners[43]. Alternatively, the key compartment may lie in the GC dendrite, with the transmission characteristics determined by the postsynaptic complement of transmitter receptors, local membrane dynamics, and AC innervation. Again, this would require that different parts of the GC dendrite operate

independently, whereas there is some evidence that salamander GCs are electrotonically compact[44]. Clearly, one would like to observe directly the activity within presynaptic terminal arbors and postsynaptic dendritic trees, and new methods of targeted optical imaging may make this possible in the near future[45]. Here we consider in more detail possible mechanisms for our specific observations.

Regarding the diversity in transmission kinetics (Figs. 2 and 3), two factors mentioned above are known to affect the time course of the GC response: Presynaptic depletion of vesicles makes for a transient postsynaptic response[20,21,32]. Feedback/feedforward inhibition from ACs can also truncate the postsynaptic response[11–13]. Interestingly, these two mechanisms react in opposite ways to the block of AC activity. The removal of tonic presynaptic inhibition will enhance transmitter release, speed depletion, and thus further shorten the response. By contrast, removal of feedback/feedforward inhibition will extend the response. Simulations of BC-GC transmission showed that a combination of synaptic depression and inhibition is indeed sufficient to produce the observed bidirectional changes in the transmission dynamics (Fig. 4).

Certain forms of contrast adaptation in the retina have been traced to a reduction of transmitter release from BCs[22–24]. This might be explained again by a process of presynaptic depletion[20,21]. Normally, the BC terminal receives tonic inhibition from ACs[31], which lowers the synaptic release and thus counteracts depletion. When inhibition is blocked, the depletion effects become more pronounced, which may explain why most BC-GC synapses become desensitizing (Fig. 5g). Alternatively, the increase in GC firing may modulate the behavior of postsynaptic conductances. This could contribute to contrast adaptation of individual connections[33,34], as long as their dendritic compartments are electrotonically separated.

Rectification is a well-known aspect of vesicle release at all synapses. However, the ribbon synapses at BC terminals are somewhat special; They allow for tonic release of glutamate and a continuous modulation of the release rate[46]. The rate increases nonlinearly with presynaptic voltage, owing largely to the voltage-dependent calcium influx[38,39]. The degree of rectification then depends on the BC resting potential and the voltage range during neural signaling. If the resting potential is high and the range is small, the modulation of the release rate may be essentially linear about the resting rate (Supplementary Fig. 3). In the present experiments the presynaptic voltage drive was deliberately large, and thus most BC-GC connections showed asymmetric effects of depolarization and hyperpolarization. Nevertheless, different synapses were clearly operating along different parts of the voltage-release curve (Fig. 7).

Finally, the gating of BC-GC transmission by distant visual stimuli (Fig. 8 and Supplementary Figs. 4 and 5) could be accomplished by presynaptic inhibition from polyaxonal ACs[17,24,40,47]. Indeed, these stimuli hyperpolarize the BC soma[17] (Supplementary Fig. 4a). Since some connections from the same BC are unaffected (Fig. 8), this view requires that certain terminals receive the inhibition and others not; the hyperpolarization at the soma then reflects an average over these inputs. The morphology of polyaxonal ACs makes such a selective connectivity plausible: They carry sparse, straight and unbranched axons[17,40,48]. As such an axon passes through a BC terminal arbor, it can contact only a few of the terminals that lie in its path. Hence different terminals will be innervated by different polyaxonal ACs, allowing for the observed diversity in gating.

Implications for retinal computation

In a simple view of neural circuits, the nerve cells are treated as the active components, with fibers and synapses merely conducting signals between them. From the present work, we

conclude that each connection between neurons in the inner plexiform layer is an active circuit element, whose transmission parameters are drawn from a broad palette of component options, and whose performance is controlled by its own microcircuit (Supplementary Fig. 6). These individual BC-GC connections may be the primitives of retinal computation, much as transistors form the primitives for an electronic computer.

What are the potential benefits for retinal functions of such a fine-grained control of visual signals? First, this organization permits a greater range of distinct visual computations to proceed in parallel. For an illustration of this principle beyond the current study, consider the ON-OFF direction-selective ganglion cells (DSGCs). These neurons fire selectively when a spot moves in one direction, but not for the opposite direction[19]. They are sensitive to tiny motions within the receptive field[49], and thus the fundamental computation happens locally, in part from presynaptic inhibition of a BC terminal by a starburst amacrine cell (SAC) dendrite. The BC itself is not direction-selective, but the SAC dendrite is, and thus the BC terminal becomes a direction-selective feature detector. Our observations (Supplementary Fig. 1) suggest that each BC contributes its terminals to DSGCs with all four directional preferences, by combining with different SAC dendrites. If instead each BC had just one type of synaptic output, then each DSGC would receive input from only a quarter of the BCs. By exploiting individual BC-GC connections as elementary feature detectors, the retina thus uses its limited resources efficiently.

Second, the independent control of the various BC-GC connections shapes the way the retina adapts to prolonged visual stimulation. Among all the BC inputs feeding a GC, any given visual stimulus will drive only a subset strongly. These connections will adapt, for example owing to the synaptic depletion discussed above, and thus the sensitivity of the GC to that prolonged stimulus gradually declines. Meanwhile the cell retains high sensitivity to novel stimuli that drive the previously dormant BC inputs. For example, a GC may desensitize to persistent stimuli with a certain orientation, while retaining high sensitivity to novel stimuli of the orthogonal orientation[50]. In general, this organization allows the retina to implement a pattern-selective adaptation that had long been thought to arise only in higher visual areas[14].

Finally, the gain of a given BC-GC connection is not only a function of its recent activity, but can be controlled by presynaptic AC circuits (Fig. 8). When this modulation affects different synapses in opposite directions, the selectivity of the receiving GC may be altered dramatically. For example, for some GCs the polarity of the light response can switch from Off-type to On-type, depending on the activity in distant ACs[40]. This suggests a flexible routing of signals from different BC pathways into one GC, and similarly from the same BC to different GCs (Fig. 8). Such fine-scale routing is an essential feature of artificial computing machines, and its full implications for neuronal circuits remain to be explored.

Methods

Electrophysiology

Simultaneous intracellular and multielectrode recording was performed as described previously[17], following protocols approved by the Institutional Animal Care and Use Committee at Harvard University. In short, the dark-adapted retina of a tiger salamander (*Ambystoma tigrinum*; both sexes; age unspecified but in the larval stage) was isolated and placed on a flat array of 61 extracellular electrodes with the ganglion cell (GC) side down (Fig. 1a). The retina was superfused with oxygenated Ringer's medium (in mM: NaCl, 110; $NaHCO_3$, 22; KCl, 2.5; $MgCl_2$, 1.6; $CaCl_2$, 1; and D-glucose, 10; equilibrated with 95% O_2 and 5% CO_2 gas) at room temperature. Sharp intracellular microelectrodes were filled with 2 M potassium acetate and 3% Rhodamine Dextran 10,000 MW (fluorescent dye; Molecular

Probes) with a final impedance of 150–250 MΩ, and blindly inserted into various cells until one with visual response characteristics matching those of bipolar cells (BCs) was found[37]. We sampled the signals from each extra- and intra-cellular electrode at 10 kHz, and used an Axoclamp 2B amplifier (Molecular Devices, Palo Alto, CA) in bridge mode for intracellular recordings and current injection into BCs. In all experiments, we alternately delivered depolarizing and hyperpolarizing square pulse currents (500 pA; 1 s each) into BCs with 2 s intervals (Fig. 1d). Each trial of this protocol thus lasted for 6 s, and each BC was typically examined with 30–100 trials. In some experiments, we also used a train of square-wave pulse currents (±500 pA; 1 Hz; 10 s) to deplete transmission from the intracellularly stimulated BC (10–15 trials with 10 s intervals; Fig. 6c–e).

Visual Stimulation

Visual stimuli were displayed on a gamma-corrected cathode-ray tube monitor (DELL E773c; frame rate 100 Hz; mean luminance ~18 mW m^{-2}) and projected on the photoreceptor layer of the retina as described previously[17]. Bipolar cells were identified during the experiment by their responses to center spot (~200 μm diameter), annulus ring (~500 μm inner diameter, ~1,000 μm outer diameter), and full-field flash stimuli. The spatio-temporal receptive fields of BCs and GCs were mapped using flickering checkerboard stimuli[51] for 10–15 minutes, with square fields 20–100 μm in width, each modulated independently by white noise (e.g., Supplementary Fig. 1).

To characterize how GC responses adapt to BC inputs (Fig. 6c–e), we stimulated the GCs in two ways: one by single BC current injection to induce adaptation in one BC pathway, and the other by visual stimulation to probe the effects on other BC pathways. The visual stimulus was comprised of black and white stripes (80 μm width) confined to an annulus region (outer diameter, 1,000 μm; inner diameter, 500 μm; centered at the BC soma), and its contrast was inverted twice (with 0.5 s interval) 3 s before and immediately after repetitive intracellular stimulation of a single BC (see above). Note that this visual stimulus did not change its mean intensity, and that it intersected with the receptive field center of the GC but not that of the current-stimulated BC.

To examine how amacrine cells (ACs) gate the synaptic transmission between BCs and GCs (Fig. 8 and Supplementary Figs. 4 and 5), the entire visual field (6,400×4,800 μm) was covered by a grating of black and white stripes (80 μm width) and divided into a circular center region (1,000 μm in diameter, centered at the BC soma) and the surrounding background region[17,24]. In combination with the current injection into a BC, the surrounding grating was then either shifted by a half period every 200 ms or jittered on every 10 ms frame update (Gaussian random motion with a standard deviation of 2 mm s^{-1}, corresponding to a step size of 2 pixels per frame) to recruit inputs from polyaxonal ACs[17,40]. The center region remained static so as not to visually stimulate the current-stimulated BC or GCs nearby. In the former shifting case, every current injection trial was delayed by 50 ms in order to vary the relative timing between the onset of square pulse currents and that of background stimulus motion. We also inverted the contrast of the center and surrounding gratings in or out of phase to examine the BC response characteristics[17] (Supplementary Fig. 4a).

Data analysis

For extracellular recordings, spike trains from individual GCs were extracted from raw voltage traces by a semi-automated spike-sorting algorithm written in Igor (Wave Metrics). In total we identified 4,236 GCs (mean spontaneous firing rate, 1.0 Hz; standard deviation, 2.2 Hz; median, 0.20 Hz), of which 965 GCs showed significant responses to single BC stimulation and thus were used for subsequent analyses. Note that the GC layer also contains

some displaced ACs, but their action potentials are expected to be below the noise level of the multielectrode recordings and are attenuated further by signal filtering prior to spike sorting[52]. The extracted spike timing data and intracellular data traces were then analyzed in Matlab (Mathworks).

Receptive field analysis—The spatio-temporal receptive fields of BCs and GCs were estimated by reverse-correlation methods[17,51]. Using the random flicker stimulus, we computed the response-weighted average of the stimulus waveform, where the weight is the measured membrane voltage for BCs (e.g., Supplementary Fig. 1a), and spike number for GCs (e.g., Supplementary Fig. 1b–e). To display the receptive field locations, we computed two-dimensional Gaussian fits to the spatial receptive field and assigned the cell's location to the center of that profile (e.g., Fig. 1c).

Effective connection strength—To quantify transmission from BCs to GCs, we first computed the peri-stimulus time histogram (PSTH; 0.1 s bin width) of GC spiking activity while manipulating BC activity intracellularly. For those GCs that had significantly different firing rates from their spontaneous activity (r_{spont}; based on the activity 1 s before the onset of current injection) in at least one bin during the current injection periods (significance level, 0.05; two-tailed with Bonferroni correction), we calculated the average firing rates for the 1 s periods of BC depolarization and hyperpolarization: r_{dep} and r_{hyp}, respectively. If the difference ($r_{dep} - r_{hyp}$) was significantly above or below zero, then we considered that the BC had sign-preserving or sign-inverting effects on the GC activity, respectively. The confidence interval was estimated by bootstrap resampling methods over trials (10,000 repeats). The effective strength of the BC-GC connection was then defined as:

$$\mathrm{ES[dep;hyp]} = \frac{r_{dep} - r_{hyp}}{\sqrt{(s_{dep}^2 + s_{hyp}^2)/2}} \quad (1)$$

where s_{dep} and s_{hyp} are the standard deviation of the GC firing rates across trials upon BC depolarization and hyperpolarization, respectively.

This standardized measure (called the "effect size" in statistics) does not depend on the data length (number of trials), unlike the *p*-values in the significance tests. Changes in ES[dep;hyp] were thus used as a measure of the effects of background visual stimulation on BC-GC connections (Fig. 8b–d). Estimation of statistical significance follows the confidence intervals of ES[dep;hyp] in the presence and absence of the background stimulation. The Levene's test (for the equality of variance) and χ^2-test (for the independence of the observed frequencies of the significant changes in ES[dep;hyp]) were used to judge the effects of the drug application across the population (Fig. 8d).

Diversity of signals from individual bipolar cells—To quantify the divergence of BC signals, we partitioned the total variation of GC response characteristics into the sum of the variation within inputs from individual BCs and the variation across different BCs, much as in the analysis of variance. Formally,

$$\begin{array}{ccccc} \sum_{i,j}(x_{ij}-x_{..})^2 & = & \sum_{i,j}(x_{ij}-x_{i.})^2 & + & \sum_{i,j}(x_{i.}-x_{..})^2 \\ \text{Total variation} & = & \text{Variation within BCs} & + & \text{Variation across BCs} \end{array} \quad (2)$$

where x_{ij} is any given response property of interest for *j*-th GC in response to *i*-th BC stimulation (for $i = 1, \ldots, n$ and $j = 1, \ldots, m_i$), and $x_{i.}$ and $x_{..}$ indicate the average over *j* and over all cell pairs, respectively. The fraction of the total variation due to the variation within

inputs from individual BCs was then computed as the ratio of the "variation within BCs" to the "total variation" from Eq.(2).

Dynamics—To analyze the dynamics of BC-GC connectivity, we fit the PSTHs of GCs in response to BC depolarization with the following unimodal function: $f(t) = \alpha t^{\beta} \exp(-t/\gamma) + r_{spont}$, where α, β, and γ denote the free parameters, t (>0) indicates the time after the onset of current injection, and r_{spont} is the spontaneous firing rate. The peak latency was then computed as $t_{peak} = \beta\gamma$ and the peak firing rate as $r_{peak} = f(t_{peak}) - r_{spont}$. Confidence intervals on the fit parameters were used for judging if significant variation exists among different BC-GC connections (Fig. 2c, d). The sign test was used to examine the changes in r_{peak} before and after drug application (Fig. 3c), and the Levene's test was used to assess the changes in the distribution of t_{peak} (Fig. 3d).

Adaptation—For those GCs with low spontaneous firing rates ($r_{spont} \leq 1$ Hz) but high peak rates ($r_{peak} \geq 5$ Hz), we analyzed the variation of the peak rate and latency across trials to examine adaptive changes in BC-GC transmission over time (Figs. 5 and 6). We first computed the peak rate and latency using a moving window of 10 trials, and performed a linear regression over trials. We then considered that the peak rate showed desensitization or sensitization if the slope was significantly below or above zero, respectively. For the peak latency, significant decrease or increase over trials indicates sensitization or desensitization, respectively. Note that the rate adaptation did not necessarily coincide with the latency adaptation (Fig. 5c, d). These slope values were used for the divergence analysis (Fig. 5e), and the χ^2-test was used for examining the effects of the inhibitory transmission blockers (Fig. 5g).

To address whether the adaptation arises before or after GCs integrate their synaptic inputs from BCs (Fig. 6), we examined if adaptation in one BC pathway (driven by single BC current injection) affects the GC responses to inputs from other BC pathways (driven by a visual stimulus). A single exponential function was used to fit the time course of GC responses to repetitive intracellular stimulation of single BCs (Fig. 6c, d). The sign test was used to compare the GC visual responses before and after the adaptation by the current injection (r_{before} and r_{after}, respectively, using the spike counts during the 1 s visual stimulation periods; Fig. 6e).

Rectification—For those GCs with sufficiently high spontaneous firing rates ($r_{spont} \geq 1$ Hz), we investigated if the BC-GC synaptic transmission was rectified or not (Fig. 7). Specifically, we used bootstrap resampling methods over trials (10,000 repeats) to analyze the differences of r_{dep} and r_{hyp} from $r_{spont.}$ We considered that the synaptic transmission was rectified if either r_{dep} or r_{hyp} was significantly different from r_{spont}, and nonrectified if both r_{dep} and r_{hyp} were significantly different from r_{spont}. The rectification index was defined as:

$$\frac{\mathrm{ES[dep;spont]} - \mathrm{ES[spont;hyp]}}{\mathrm{ES[dep;spont]} + \mathrm{ES[spont;hyp]}} \quad (3)$$

where ES[dep;spont] and ES[spont;hyp] from Eq.(1) indicate the effective strength of BC depolarization and hyperpolarization, respectively (Fig. 7b, d). Note that ES[dep;spont] > 0 for an increase in GC spiking activity on BC depolarization, while ES[spont;hyp] > 0 for a decrease in GC spiking activity on BC hyperpolarization. The index is thus close to unity for rectifying excitatory transmission because ES[dep;spont] > 0 and ES[spont;hyp] ≈ 0, whereas the index is near zero for nonrectifying transmission because ES[dep;spont] ≈ ES[spont;hyp]. The rank-sum test (for the equality of median rectification indices) and the χ^2-test (for the independence of the observed frequencies of rectifying and nonrectifying

BC-GC connections) were used to judge the effects of blocking inhibitory AC circuits (Fig. 7d).

Simulation

To examine the contributions of different AC circuits to the transmission dynamics from BCs to GCs (Fig. 3), we incorporated the following four types of AC inputs into a phenomenological model of the synaptic transmission[53] (Fig. 4 and Supplementary Fig. 7); tonic presynaptic inhibition ($\alpha_{pre} > 0$), tonic postsynaptic inhibition ($\alpha_{post} > 0$), feedback presynaptic inhibition ($\beta_{pre} > 0$), and feedforward postsynaptic inhibition ($\beta_{post} > 0$). Specifically, the presynaptic side was modeled by the dynamics of the vesicle pool $x \in [0,1]$ and release rate $u \in [0,1]$:

$$\frac{dx}{dt} = \frac{1-x}{\tau_d} - v \quad (3)$$

$$\frac{du}{dt} = \frac{u_0-u}{\tau_f} + k(1-u)V_m \quad (4)$$

where τ_d and τ_f are the recovery constants of depression and facilitation, respectively. The release rate u works as a driving force of vesicle release, reflecting, for example, the fraction of opened calcium channels[20,32]; u_0 and k indicate the baseline and the change rate of u, respectively. The effective presynaptic membrane potential $V_m = V(I) - \alpha_{pre} - B_{pre}$ changes upon receiving input current I with current-voltage transform V. When $V_m > 0$, neurotransmitters are released by the amount $v = [uxV_m]_+$ as in Eq.(4), where $[\cdot]_+$ is a half-wave rectification function, and the release rate u increases because a fraction of closed calcium channels ($1 - u$) opens as in Eq.(5). With time constant τ, the released vesicles v recruit feedback or feedforward inhibition: $dB_*/dt = -B_*/\tau + v\beta_*$, where "$*$" is either "pre" or "post", respectively. The postsynaptic dynamics were then simulated by the firing rate $r = [v - \theta]_+$, where $\theta = \theta_0 + \alpha_{post} + B_{post}$ is the effective spiking threshold with a baseline of θ_0. Note that GCs in the salamander retina are thought to be electrotonically compact for excitatory input[44]; and that voltage-dependent processing in the dendrites contributes little to signal integration[33].

The simulation was done at time steps of 1 ms using the following parameter values. For simplicity, we ignored the nonlinear effects of current-voltage transform in BCs[54] and assumed $V(I) = IR_{in} + V_0$ with an input resistance R_{in} = 100 MΩ and a baseline potential V_0 = 0 mV. In accord with our experimental protocol, we used I = 500 pA for $t \in [0,1]$, otherwise 0 A. Previous studies suggest that recovery from synaptic depression after a sustained depolarization is slow[32], whereas the calcium dynamics are relatively fast and facilitatory[55] and the time course of retinal inhibition is even faster[56]. Thus we used τ_d = 5 s, τ_f = 0.5 s, $u_0 = k$ = 0.01, and τ = 0.1 s. For the postsynaptic side, we set θ_0 = 0.8 so that the normalized firing rate r decays within ~0.5 s in the absence of inhibition (Fig. 3). For the inhibition parameters, we used $\alpha_{pre} \in [0,3]$; $\alpha_{post} \in [0,0.18]$; $\beta_{pre} \in [0,0.75]$; and $\beta_{post} \in [0,1.5]$ (normalized in Fig. 4 for display purposes). A stronger inhibition led to no firing responses in the postsynaptic side. We obtained qualitatively similar results over many different sets of the parameters, confirming that the model is robust in accounting for the effects of AC circuitry.

To examine how the rectification arises (Fig. 7), we also simulated the transmitter release v at different baseline potentials V_0 (Supplementary Fig. 3). Specifically, we used V_0 = 0, 7.5, and 15 mV with the injected current I following the protocol of Fig. 1d, and ran the

simulation with the same parameter values as described above but with no inhibition (a_{pre} = a_{post} = β_{pre} = β_{post} = 0).

Supplementary Material

Refer to Web version on PubMed Central for supplementary material.

Acknowledgments

We gratefully acknowledge Ed Soucy for his extensive help in experiments, as well as all the members of the Meister laboratory for many useful discussions.

Grants: This work was supported by a JSPS Postdoctoral Fellowship for Research Abroad (H.A.) and grants from NIH (M.M.).

References

1. Wässle H. Parallel processing in the mammalian retina. Nat Rev Neurosci. 2004; 5:747–757. [PubMed: 15378035]
2. Masland RH. The fundamental plan of the retina. Nat Neurosci. 2001; 4:877–886. [PubMed: 11528418]
3. Wu SM, Gao F, Maple BR. Functional architecture of synapses in the inner retina: segregation of visual signals by stratification of bipolar cell axon terminals. J Neurosci. 2000; 20:4462–4470. [PubMed: 10844015]
4. Ghosh KK, Bujan S, Haverkamp S, Feigenspan A, Wässle H. Types of bipolar cells in the mouse retina. J Comp Neurol. 2004; 469:70–82. [PubMed: 14689473]
5. Roska B, Molnar A, Werblin FS. Parallel processing in retinal ganglion cells: how integration of space-time patterns of excitation and inhibition form the spiking output. J Neurophysiol. 2006; 95:3810–3822. [PubMed: 16510780]
6. Boycott BB, Wässle H. Morphological classification of bipolar cells of the primate retina. Eur J Neurosci. 1991; 3:1069–1088. [PubMed: 12106238]
7. Awatramani GB, Slaughter MM. Origin of transient and sustained responses in ganglion cells of the retina. J Neurosci. 2000; 20:7087–7095. [PubMed: 10995856]
8. Mariani AP. Bipolar cells in monkey retina selective for the cones likely to be blue-sensitive. Nature. 1984; 308:184–186. [PubMed: 6199677]
9. Slaughter MM, Miller RF. 2-amino-4-phosphonobutyric acid: a new pharmacological tool for retina research. Science. 1981; 211:182–185. [PubMed: 6255566]
10. DeVries SH. Bipolar cells use kainate and AMPA receptors to filter visual information into separate channels. Neuron. 2000; 28:847–856. [PubMed: 11163271]
11. Tachibana M, Kaneko A. Retinal bipolar cells receive negative feedback input from GABAergic amacrine cells. Vis Neurosci. 1988; 1:297–305. [PubMed: 2856476]
12. Nirenberg S, Meister M. The light response of retinal ganglion cells is truncated by a displaced amacrine circuit. Neuron. 1997; 18:637–650. [PubMed: 9136772]
13. Dong CJ, Werblin FS. Temporal contrast enhancement via $GABA_C$ feedback at bipolar terminals in the tiger salamander retina. J Neurophysiol. 1998; 79:2171–2180. [PubMed: 9535976]
14. Gollisch T, Meister M. Eye smarter than scientists believed: Neural computations in circuits of the retina. Neuron. 2010; 65:150–164. [PubMed: 20152123]
15. Enroth-Cugell C, Freeman AW. The receptive-field spatial structure of cat retinal Y cells. J Physiol. 1987; 384:49–79. [PubMed: 3656154]
16. Demb JB, Zaghloul K, Haarsma L, Sterling P. Bipolar cells contribute to nonlinear spatial summation in the brisk-transient (Y) ganglion cell in mammalian retina. J Neurosci. 2001; 21:7447–7454. [PubMed: 11567034]
17. Baccus SA, Ölveczky BP, Manu M, Meister M. A retinal circuit that computes object motion. J Neurosci. 2008; 28:6807–6817. [PubMed: 18596156]

18. Enroth-Cugell C, Robson JG. The contrast sensitivity of retinal ganglion cells of the cat. J Physiol. 1966; 187:517–552. [PubMed: 16783910]
19. Demb JB. Cellular mechanisms for direction selectivity in the retina. Neuron. 2007; 55:179–186. [PubMed: 17640521]
20. Burrone J, Lagnado L. Synaptic depression and the kinetics of exocytosis in retinal bipolar cells. J Neurosci. 2000; 20:568–578. [PubMed: 10632586]
21. Singer JH, Diamond JS. Vesicle depletion and synaptic depression at a mammalian ribbon synapse. J Neurophysiol. 2006; 95:3191–3198. [PubMed: 16452253]
22. Jarsky T, et al. A synaptic mechanism for retinal adaptation to luminance and contrast. J Neurosci. 2011; 31:11003–11015. [PubMed: 21795549]
23. Oesch NW, Diamond JS. Ribbon synapses compute temporal contrast and encode luminance in retinal rod bipolar cells. Nat Neurosci. 2011; 14:1555–1561. [PubMed: 22019730]
24. Ölveczky BP, Baccus SA, Meister M. Retinal adaptation to object motion. Neuron. 2007; 56:689–700. [PubMed: 18031685]
25. Wässle H, Puller C, Müller F, Haverkamp S. Cone contacts, mosaics, and territories of bipolar cells in the mouse retina. J Neurosci. 2009; 29:106–117. [PubMed: 19129389]
26. Zhang AJ, Wu SM. Receptive fields of retinal bipolar cells are mediated by heterogeneous synaptic circuitry. J Neurosci. 2009; 29:789–797. [PubMed: 19158304]
27. Zhang A-J, Wu SM. Responses and receptive fields of amacrine cells and ganglion cells in the salamander retina. Vision Res. 2010; 50:614–622. [PubMed: 20085780]
28. Arai I, Tanaka M, Tachibana M. Active roles of electrically coupled bipolar cell network in the adult retina. J Neurosci. 2010; 30:9260–9270. [PubMed: 20610761]
29. Mittman S, Taylor WR, Copenhagen DR. Concomitant activation of two types of glutamate receptor mediates excitation of salamander retinal ganglion cells. J Physiol. 1990; 428:175–197. [PubMed: 2172521]
30. Lukasiewicz PD, Lawrence JE, Valentino TL. Desensitizing glutamate receptors shape excitatory synaptic inputs to tiger salamander retinal ganglion cells. J Neurosci. 1995; 15:6189–6199. [PubMed: 7666201]
31. Jones SM, Palmer MJ. Activation of the tonic $GABA_C$ receptor current in retinal bipolar cell terminals by nonvesicular GABA release. J Neurophysiol. 2009; 102:691–699. [PubMed: 19494193]
32. von Gersdorff H, Matthews G. Depletion and replenishment of vesicle pools at a ribbontype synaptic terminal. J Neurosci. 1997; 17:1919–1927. [PubMed: 9045721]
33. Kim KJ, Rieke F. Temporal contrast adaptation in the input and output signals of salamander retinal ganglion cells. J Neurosci. 2001; 21:287–299. [PubMed: 11150346]
34. Kim KJ, Rieke F. Slow Na^+ inactivation and variance adaptation in salamander retinal ganglion cells. J Neurosci. 2003; 23:1506–1516. [PubMed: 12598639]
35. Kastner DB, Baccus SA. Coordinated dynamic encoding in the retina using opposing forms of plasticity. Nat Neurosci. 2011; 14:1317–1322. [PubMed: 21909086]
36. Rieke F. Temporal contrast adaptation in salamander bipolar cells. J Neurosci. 2001; 21:9445–9454. [PubMed: 11717378]
37. Baccus SA, Meister M. Fast and slow contrast adaptation in retinal circuitry. Neuron. 2002; 36:909–919. [PubMed: 12467594]
38. Heidelberger R, Heinemann C, Neher E, Matthews G. Calcium dependence of the rate of exocytosis in a synaptic terminal. Nature. 1994; 371:513–515. [PubMed: 7935764]
39. Matsui K, Hosoi N, Tachibana M. Excitatory synaptic transmission in the inner retina: paired recordings of bipolar cells and neurons of the ganglion cell layer. J Neurosci. 1998; 18:4500–4510. [PubMed: 9614227]
40. Geffen MN, de Vries SEJ, Meister M. Retinal ganglion cells can rapidly change polarity from Off to On. PLoS Biol. 2007; 5:e65. [PubMed: 17341132]
41. Roska B, Nemeth E, Werblin FS. Response to change is facilitated by a three-neuron disinhibitory pathway in the tiger salamander retina. J Neurosci. 1998; 18:3451–3459. [PubMed: 9547252]

42. Dowling JE, Werblin FS. Synaptic organization of the vertebrate retina. Vision Res Suppl. 1971; 3:1–15.
43. Brandstätter JH, Koulen P, Kuhn R, van der Putten H, Wässle H. Compartmental localization of a metabotropic glutamate receptor (mGluR7): two different active sites at a retinal synapse. J Neurosci. 1996; 16:4749–4756. [PubMed: 8764662]
44. Taylor WR, Mittman S, Copenhagen DR. Passive electrical cable properties and synaptic excitation of tiger salamander retinal ganglion cells. Vis Neurosci. 1996; 13:979–990. [PubMed: 8903038]
45. Dreosti E, Esposti F, Baden T, Lagnado L. In vivo evidence that retinal bipolar cells generate spikes modulated by light. Nat Neurosci. 2011; 14:951–952. [PubMed: 21706020]
46. Lagnado L, Gomis A, Job C. Continuous vesicle cycling in the synaptic terminal of retinal bipolar cells. Neuron. 1996; 17:957–967. [PubMed: 8938127]
47. Cook PB, McReynolds JS. Lateral inhibition in the inner retina is important for spatial tuning of ganglion cells. Nat Neurosci. 1998; 1:714–719. [PubMed: 10196588]
48. Famiglietti EV. Polyaxonal amacrine cells of rabbit retina: morphology and stratification of PA1 cells. J Comp Neurol. 1992; 316:391–405. [PubMed: 1577992]
49. Barlow HB, Levick WR. The mechanism of directionally selective units in rabbit's retina. J Physiol. 1965; 178:477–504. [PubMed: 5827909]
50. Hosoya T, Baccus SA, Meister M. Dynamic predictive coding by the retina. Nature. 2005; 436:71–77. [PubMed: 16001064]
51. Meister M, Pine J, Baylor DA. Multi-neuronal signals from the retina: acquisition and analysis. J Neurosci Methods. 1994; 51:95–106. [PubMed: 8189755]
52. Segev R, Goodhouse J, Puchalla J, Berry MJ. Recording spikes from a large fraction of the ganglion cells in a retinal patch. Nat Neurosci. 2004; 7:1154–1161. [PubMed: 15452581]
53. Tsodyks M, Pawelzik K, Markram H. Neural networks with dynamic synapses. Neural Comput. 1998; 10:821–835. [PubMed: 9573407]
54. Mao BQ, MacLeish PR, Victor JD. The intrinsic dynamics of retinal bipolar cells isolated from tiger salamander. Vis Neurosci. 1998; 15:425–438. [PubMed: 9685196]
55. Kaneko A, Pinto LH, Tachibana M. Transient calcium current of retinal bipolar cells of the mouse. J Physiol. 1989; 410:613–629. [PubMed: 2552084]
56. Eggers ED, Lukasiewicz PD. Receptor and transmitter release properties set the time course of retinal inhibition. J Neurosci. 2006; 26:9413–9425. [PubMed: 16971525]

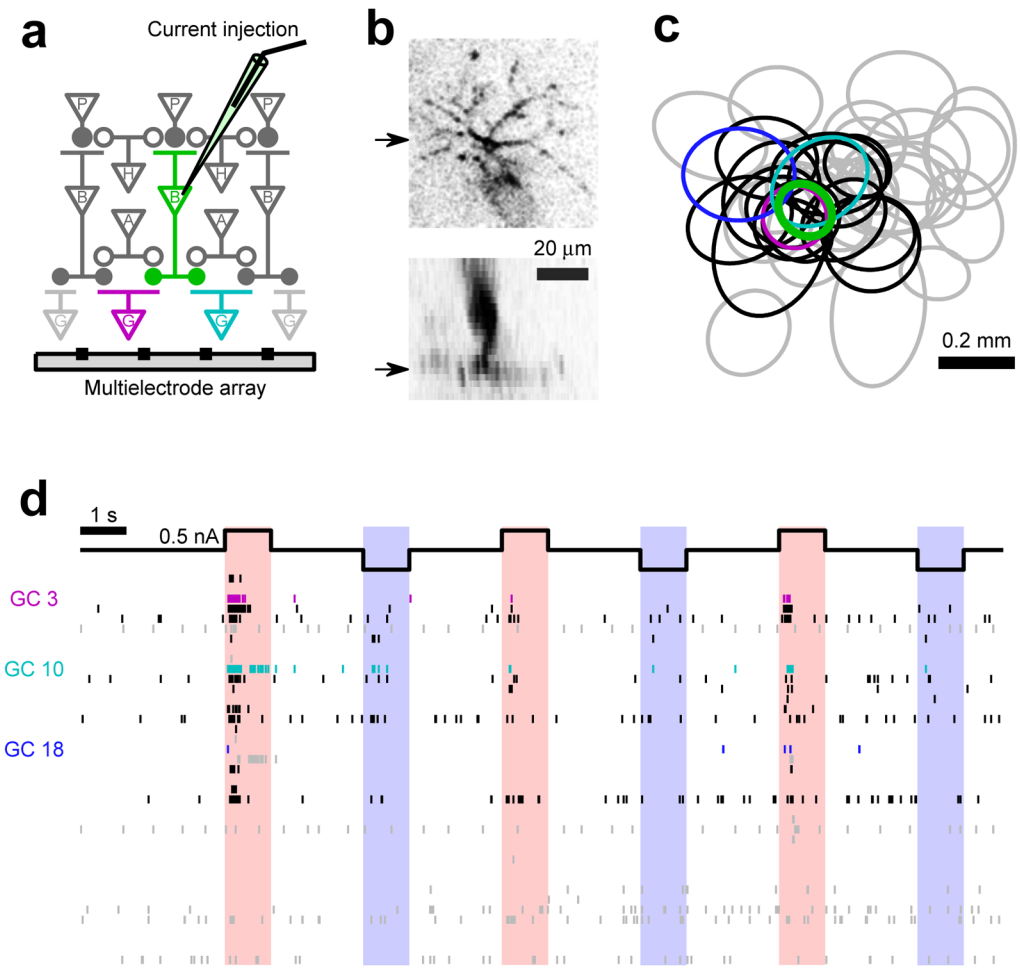

Figure 1. Many ganglion cells respond to input from a single bipolar cell

(a) Schematic diagram of the experiment. A single bipolar cell (BC) is impaled with a sharp electrode and intracellularly stimulated by current injection (see **d** for example), while a population of ganglion cells (GCs) is simultaneously recorded with a multielectrode array. A, amacrine cell (AC); B, BC; G, GC; H, horizontal cell; P, photoreceptor; filled circle, excitatory synapse; open circle, inhibitory synapse.

(b) Horizontal view of a BC, focusing on the axon arbors in the inner plexiform layer (top), and the vertical view across the soma (bottom). The arrows indicate locations of the image slices shown in the other panels, respectively.

(c) The receptive field centers of an intracellularly recorded BC (green) and of 39 GCs on the electrode array (gray, unconnected; black, cyan, purple, and blue, connected; see **d** for connectivity analysis). Each outline represents a two-dimensional Gaussian fit to the receptive field profile (contour at one standard deviation; see Supplementary Fig. 1 for details).

(d) Raster graph of GC spikes in response to inputs from a single BC (from **c**). Each row represents the spiking activity of a single GC, arranged in order of increasing distance from the BC (top to bottom). Either depolarizing (pink-shaded periods) or hyperpolarizing (blue-shaded periods) current pulses were delivered to the BC intracellularly (top trace; only the first three trials are shown here; see Supplementary Fig. 1 for more). The three representative GCs from **c** are shown in the respective colors.

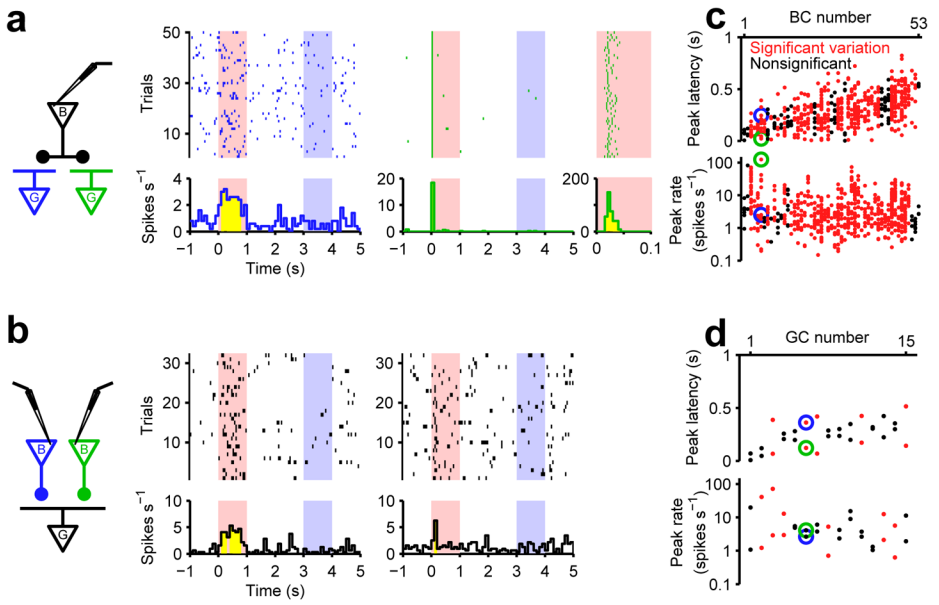

Figure 2. Individual pairs of bipolar and ganglion cells have distinct transmission properties

(a) Responses of two GCs (top, raster graphs; bottom, peri-stimulus time histogram; yellow bins, significant deviation from spontaneous firing rate) to current stimulation of a single BC. Here and in subsequent figures the current stimulus is color coded (pink/blue) as in Fig 1d. Note sustained firing in one GC (left) but very transient firing in another (middle; magnified in the right panel).

(b) Responses of a single GC to current stimulation of two different BCs (left and right; displayed as in **a**).

(c) Population data for synaptic connections divergent from the same BC. Each dot represents a BC-GC connection (one column for each BC). *Top*: Peak latency evoked by BC depolarization (0.28±0.15 s, mean ± standard deviation from 633 GC responses total). Significant variation was found in GC responses to 38 out of 53 BCs (red). The variation among the connections of individual BCs explains 62% of the total variation, whereas the variation across different BCs explains only 38% (see Methods). *Bottom:* For the peak firing rate (6.6±11.0 spikes s^{-1}), significantly different GC responses were found in 43 BCs. The variation within connections from the same BC explains 67% of the total variation.

(d) Population data for synaptic connections convergent on the same GC (displayed as in **c**). Inputs from different BCs can drive the same GC differently (5 out of 15 GCs for peak latency; 6 GCs for peak rate), and distinct dynamics can arise even with the same evoked firing rate (as in **b**, indicated by blue and green circles).

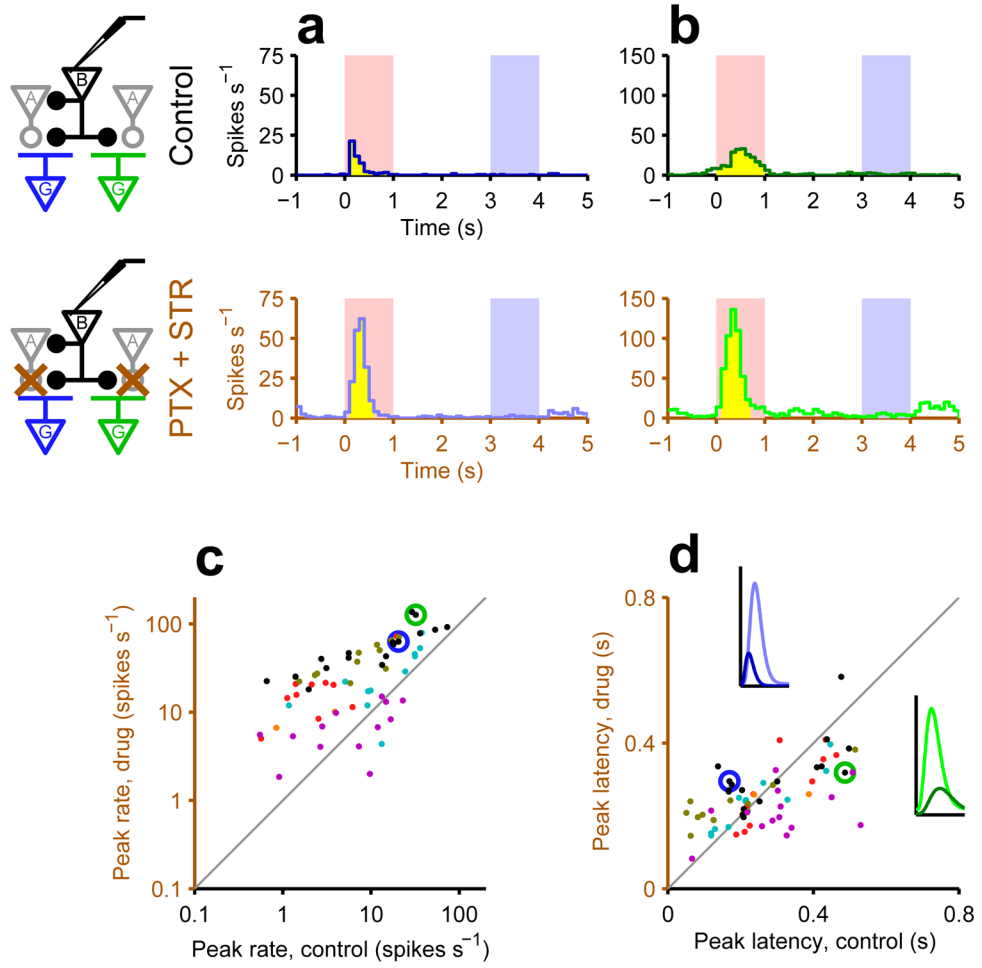

Figure 3. Dynamics of bipolar cell signals are diversified by amacrine circuits

(a, b) Spiking response of two GCs to current stimulation of a BC, with (top) and without (bottom) inputs from ACs. After blocking AC signals by 100 μM picrotoxin (PTX) and 1.0 μM strychnine (STR), the transient burst of spikes in one GC became considerably stronger and peaked later (**a**), whereas the sustained response in the other GC became stronger but peaked earlier (**b**).

(c, d) Summary of the effects of blocking inhibitory synaptic transmission on the peak firing rate (**c**) and the peak latency (**d**) evoked by single BC depolarization. Scatter plots compare the GC responses with (abscissa) and without (ordinate) inhibitory transmission (66 GCs in total from 6 BCs indicated by different colors; blue and green circles indicate those in **a** and **b**, respectively). With the inhibitory circuits active, the peak firing rate was lower (**c**; $p<0.001$, sign-test; control, 12.4±13.7 spikes s^{-1}; drug, 32.7±29.1 spikes s^{-1}; mean ± standard deviation) but there was a greater range in the peak latency (**d**; $p<0.001$, Levene's test; control, 0.27±0.13 s; drug, 0.26±0.09 s). In all six experiments, blocking AC signals made sustained responses more transient and transient responses more sustained. Insets in **d** correspond to curve fits for the examples in **a** (dark and light blue) and **b** (dark and light green).

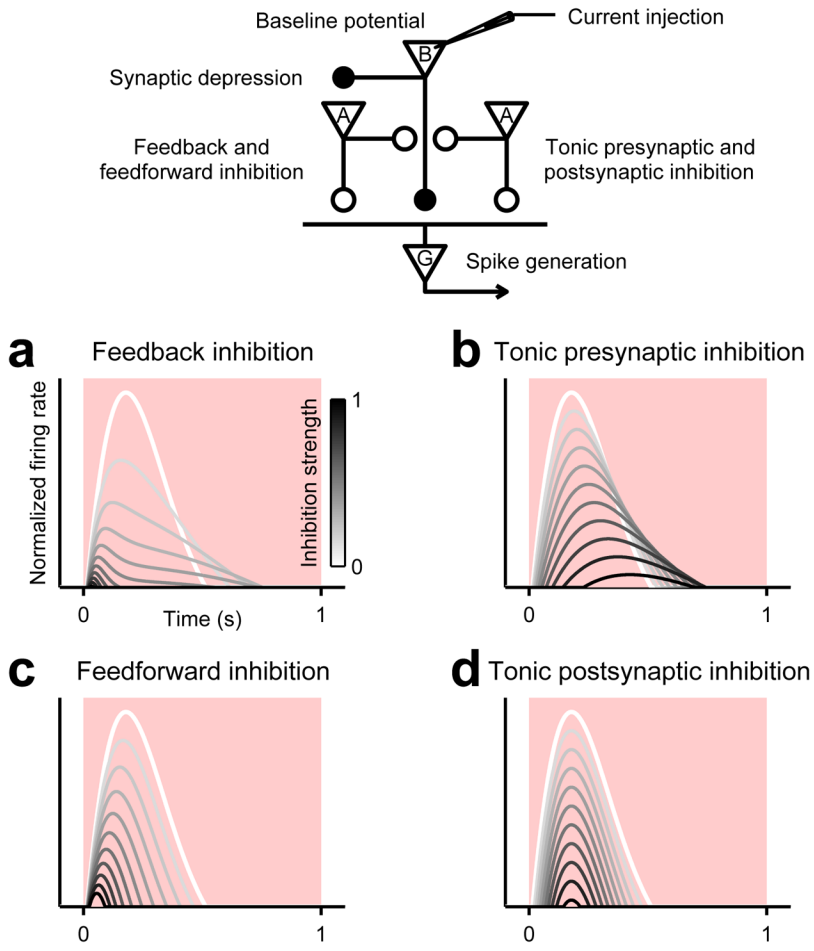

Figure 4. Interactions with amacrine cells can control the kinetics of connections between bipolar and ganglion cells

We simulated how a step change in the input current to a BC is transduced into an evoked GC firing rate in the presence of four distinct types of AC inputs (see top circuit diagram and Methods): tonic presynaptic inhibition of the BC terminal (**b**), tonic postsynaptic inhibition of the GC (**d**), feedback presynaptic inhibition (**a**), and feedforward postsynaptic inhibition (**c**). For all four types of inhibitory interactions, the evoked firing rate decreases as the inhibitory effects become stronger (trace color from white to black; see Supplementary Fig. 3 for the effects of BC baseline potential). However, the effects on the response kinetics vary (compare to experiments in Fig. 3). Tonic presynaptic inhibition prevents synaptic depletion and thus extends the GC response in time (**b**). Tonic postsynaptic inhibition affects the spiking threshold but not the release dynamics of BC terminals, and thus the peak latency remains unchanged (**d**). Both feedback presynaptic inhibition (**a**) and feedforward postsynaptic inhibition (**c**) shorten the GC responses by truncating the later component of the excitation. They differ, however, in that presynaptic inhibition slows vesicle release and thus prevents rapid synaptic depression, producing weaker but prolonged postsynaptic responses over an intermediate regime.

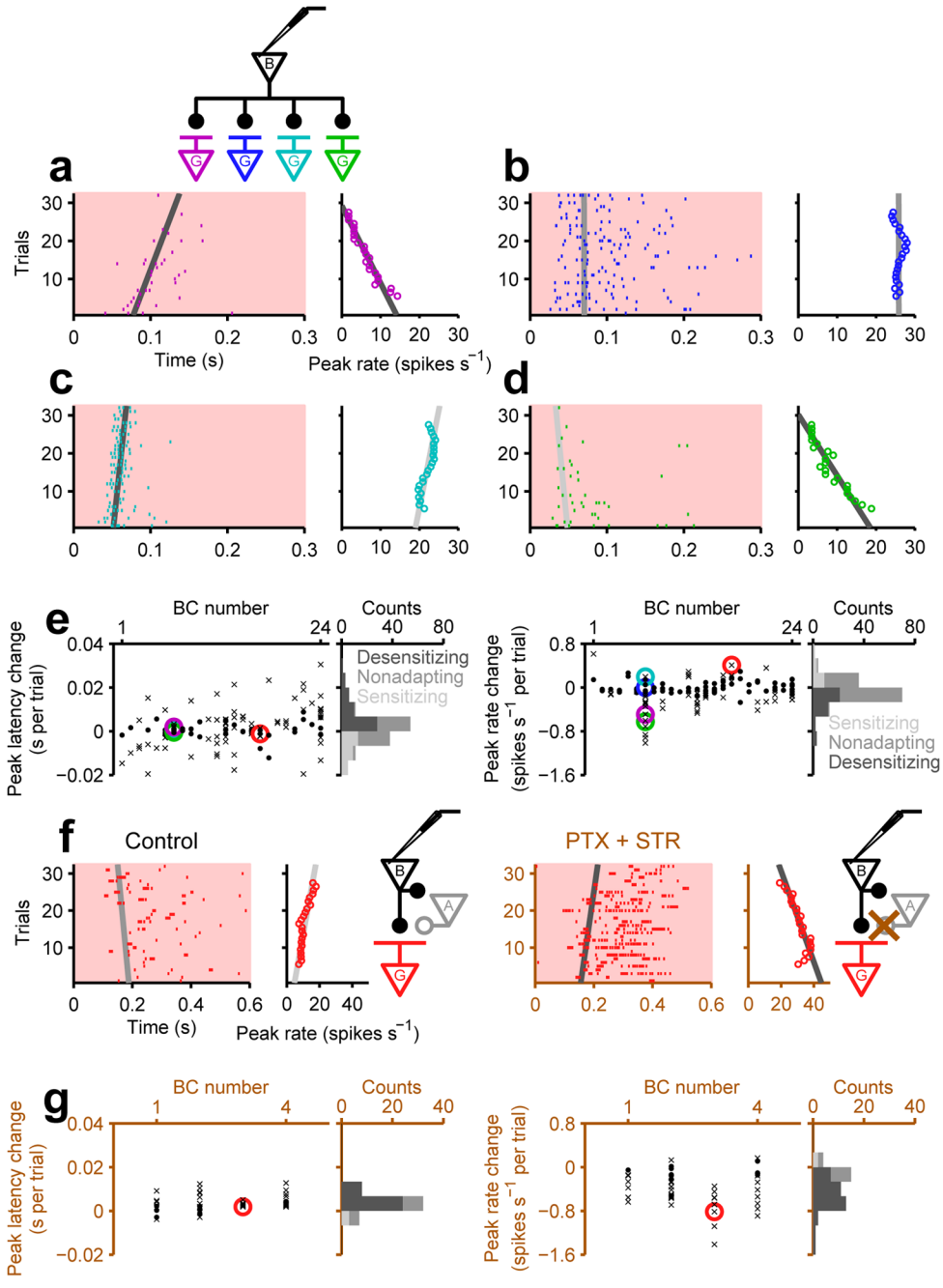

Figure 5. Adaptation of bipolar cell signals depends on interaction with amacrine cells

(a–d) Responses of four simultaneously recorded GCs to depolarization of a single BC, and their evolution over trials. **a**, *left*: Raster graph showing spikes during the first 300 ms of depolarizing current, delivered in many successive 6-s-long trials (Fig. 1d); gray line is a linear fit to the peak latency over trials (gray, nonsignificant change; dark gray, significant increase or desensitization; light gray, significant decrease or sensitization). **a**, *right*: Variation of the peak firing rate over trials with a linear fit. **b–d**: Responses of three additional GCs with different characteristics (displayed as in **a**).

(e) Population data for the slow changes in the peak latency (left) and peak rate (right). Each data point represents the adapting behavior of one BC-GC connection, estimated by the

slopes of the linear fits as in **a–d** (cross, significant change; dot, nonsignificant change; colored circles indicate those from **a–d** and **f).** Each column shows the connections of one BC (sorted in order of increasing mean latency changes). The stacked histograms are obtained from 129 BC-GC connections in total (gray, nonsignificant change; dark gray, significant desensitization; light gray, significant sensitization). For latency adaptation, 20 out of 24 BCs showed significant variation among their BC-GC connections, and this variation originating from individual BCs explains 85% of the total variation. For peak rate adaptation, 14 BCs showed significant variation and that accounts for 59% of the total.

(f) Spiking responses of a GC to BC depolarization before (left) and after (right) pharmacological block of AC signals by 100 μM picrotoxin (PTX) and 1.0 μM strychnine (STR). Displayed as in **a–d**.

(g) Population data (57 GCs total) for the adapting changes in the peak latency and peak rate over trials in absence of AC transmission (displayed as in **e**). After the block of AC signals, GCs showed desensitization more frequently for both the latency ($p<0.002$; χ^2-test) and the peak rate ($p<0.002$; χ^2-test).

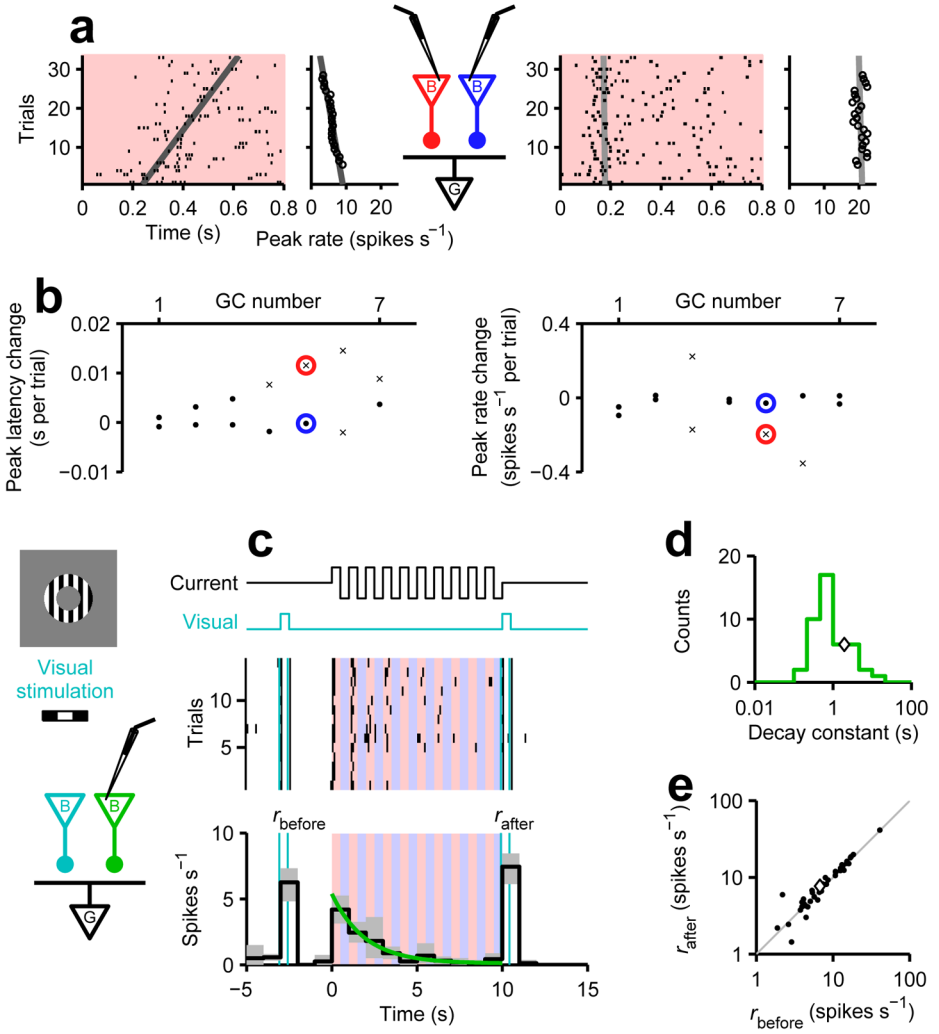

Figure 6. Adaptation is specific to individual pairs of bipolar and ganglion cells

(a) Responses of a single GC to depolarization of two different BCs (displayed as in Fig. 5a). The response to one BC showed strong desensitization over time (left), whereas that to another BC did not, despite a higher peak firing rate (right).

(b) Population data for the slow changes in peak firing rate and latency evoked by depolarization of two different BCs (displayed as in Fig. 5e; colored circles indicate those in **a**). Inputs from different BCs can lead to different adapting behaviors in the same GCs (4 out of 7 GCs for the peak latency change; 3 GCs for the peak rate change).

(c) Responses of a GC to two different inputs: current injected into a BC (top, black trace) and visual stimulation in an annulus that does not drive the injected BC (cyan; contrast-reversal grating). The GC fired on BC depolarization (middle, raster graph). This response declined over subsequent current stimulations (bottom, PSTH; gray, 95% confidence interval; green, single exponential fit). The GC also fired on the visual stimulation, both before (r_{before}) and after (r_{after}) the current injection.

(d, e) Results from many such experiments (6 BCs and 44 GCs; diamonds indicate the example in **c**). Most GCs showed desensitization in response to consecutive BC depolarizations (**d**, histogram of decay constants for an exponential fit as in **c**). This, however, did not affect the GC's responses to other BCs driven by the visual stimulus (**e**; $p>0.06$, sign-test).

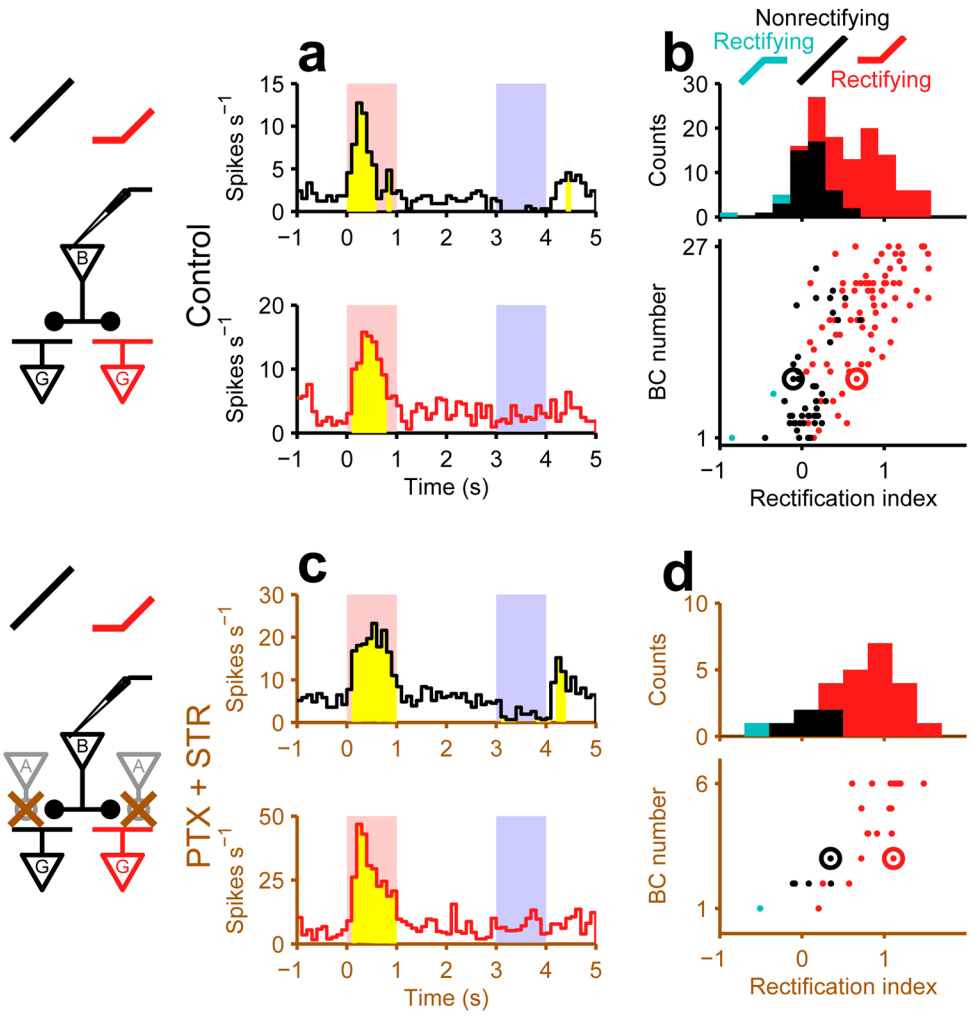

Figure 7. Rectifying and nonrectifying transmission from bipolar cells

(a) Response of two simultaneously recorded GCs to current injection of a single BC. One GC responded to both BC depolarization and hyperpolarization with opposite sign (top; "nonrectifying" transmission, black) and showed a rebound response at the end of the hyperpolarization (Supplementary Fig. 3). In contrast, the other GC responded only to the depolarization (bottom; "rectifying" transmission, red) and did not show the rebound response.

(b) Population results of rectification index from many such paired recordings (0.50±0.48, mean ± standard deviation from 127 GCs in total; see Methods for details). *Bottom*: Each dot represents one BC-GC connection (black and red circles from **a**), and each row corresponds to one BC. *Top*: Stacked histogram across all BC-GC connections (black, "nonrectifying" connections; red and cyan, "rectifying" connections transmitting primarily on BC depolarization or on hyperpolarization, respectively). Both types of connections were found in GC responses to 17 out of 27 BCs (such as in **a**). The variation of the index within individual BCs accounted for 41% of the total variation.

(c) Response of two GCs to a single BC under pharmacological block of inhibitory transmission (displayed as in **a** but a different pair from **a**).

(d) Population results of rectification tested without AC signaling (25 GCs in total). Despite an increase in the evoked firing rates (Fig. 3c), the inhibitory transmission blockers did not

significantly change the rectification index (p>0.06; rank-sum) or the observed frequencies of rectifying and nonrectifying connections across the populations (p>0.6; χ^2-test).

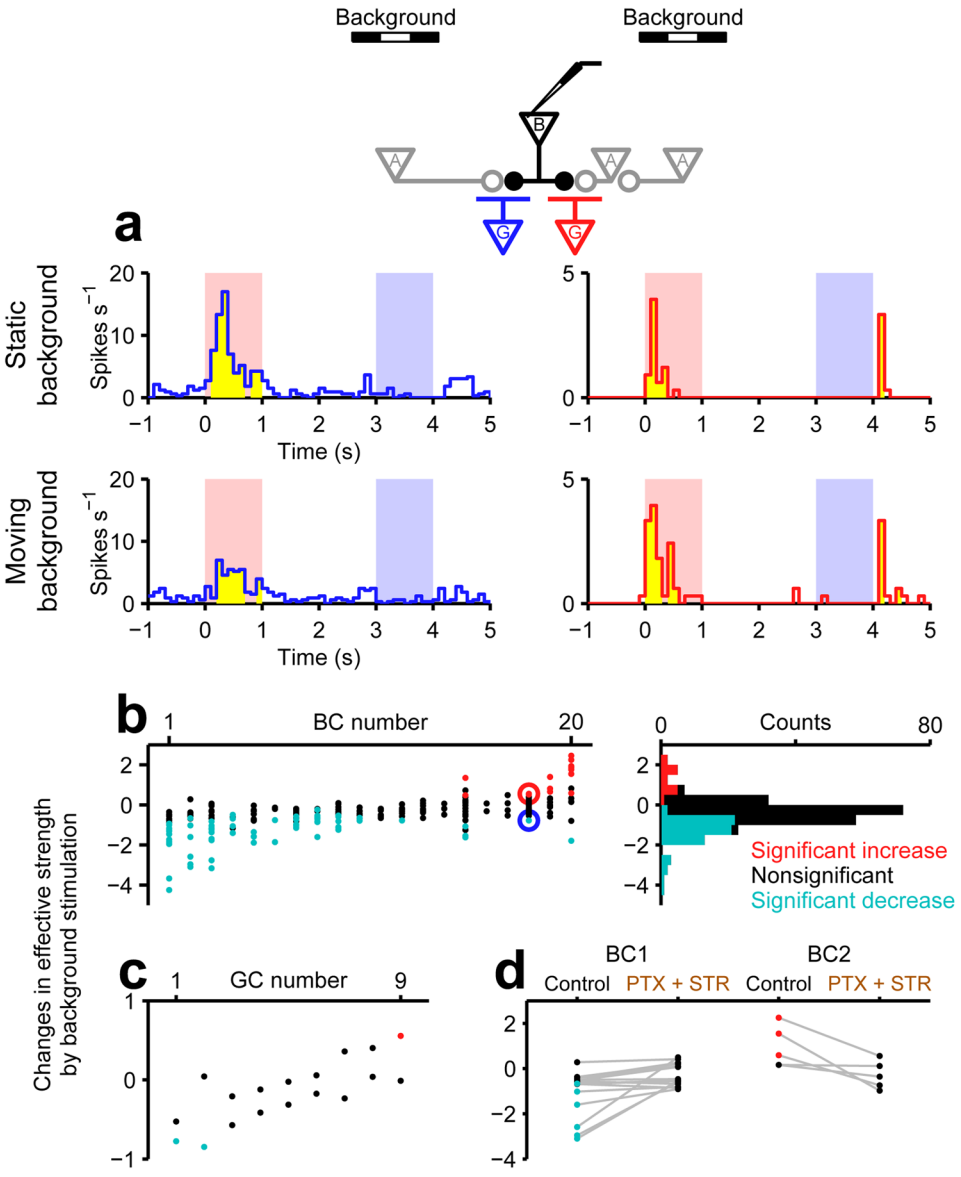

Figure 8. Amacrine cells can gate individual bipolar cell signals

(a) Response of two GCs to BC stimulation alone (top) or in conjunction with visual stimulation in a distant annulus (bottom). The visual stimulus served to drive lateral AC circuits (see top circuit diagram and Methods). Under these conditions the response of one GC to the central BC was suppressed (left), whereas that of the other GC was enhanced (right).

(b) Changes in effective strength of BC-GC connections elicited by distant visual stimulation (−0.47±0.87; mean ± standard deviation from 221 GCs in total). *Left*: Each dot represents a BC-GC connection (colored circles from **a**), and each column is one BC. 15 out of 20 BCs showed distinct modulations among their connections. This variation from individual BC signals accounted for 59% of the total variation. *Right*: stacked histogram across all connections. Background stimulation weakened 65 connections (cyan; see left side of the circuit diagram at top) but strengthened 15 connections (red; right side).

(c) The effects of background stimulation on convergent connections from two different BCs. Display as in **b**, but columns correspond to individual GCs. In 3 of 9 cases, the two

BC-GC connections experienced significantly different gating (see Supplementary Fig. 4 for an example).

(d) The effects of background visual stimulation on the transmission from central BCs to GCs before (left) and after (right) applying inhibitory transmission blockers. The drug application eliminated both the suppressive and facilitatory gating effects ($p<0.007$, χ^2-test; $p<0.02$, Levene's test; see Supplementary Fig. 5 for an example).